Precision measurements of cyclotron masses and Fermi velocities in the noble metals by the de Haas–van Alphen effect

B. Lengeler, W. R. Wampler,* R. R. Bourassa,† K. Mika, K. Wingerath, and W. Uelhoff
Institut für Festkörperforschung der Kernforschungsanlage Jülich, D5179 Jülich, Germany
(Received 21 January 1977)

A total of 54 cyclotron masses have been determined with great precision from the temperature dependence of the de Haas–van Alphen (dHvA) amplitudes in the noble metals Cu, Ag, and Au. The accuracy of the data is ±0.3%. Special care was given to the temperature and amplitude measurements. In particular the influence of magnetic interaction and of the incomplete penetration of the modulation field into the high-purity samples, which were among the most serious sources of systematic errors, were eliminated. The mass data were deconvoluted to get values of the electron velocities $v^*(\vec{k})$ for each point on the Fermi surfaces. The qualitative behavior of $v^*(\vec{k})$ agrees with that found in previous works, but the absolute values differ by as much as 10%. Local values of the electron-phonon enhancement factor, $1+\lambda(\vec{k})$, were obtained in Cu by comparing velocities deduced from dHvA cyclotron masses which include electron-phonon renormalization with band velocities deduced from a band-structure calculation. Cyclotron masses were calculated for about 40 orbits not measured in each of the three metals. The coefficient of electronic specific heat was calculated from the experimental data. The agreement with the data obtained from specific-heat measurements is excellent.

I. INTRODUCTION

The Fermi surfaces of the noble metals Cu, Ag, and Au have been studied in considerable detail by the de Haas–van Alphen effect (dHvA). A review of the data up to 1971 is given by Cracknell.[1] Later improvements of the data are the measurements by Bosacchi *et al.*[2] and by Coleridge *et al.*[3] Halse[4] has given an analytical representation of the Fermi surfaces in the form of a symmetrized Fourier series. The radius vectors of the Fermi surfaces calculated from this representation are accurate to within 0.2%. In recent years the dHvA effect has been used more and more to determine the scattering rates of the conduction electrons in dilute alloys.[5] For this kind of analysis one needs, besides the geometry of the Fermi surface, accurate data of the cyclotron masses and of the Fermi velocities. Masses have been measured by cyclotron resonance by Koch *et al.*[6] for Cu, by Howard[7] for Ag and by Langenberg *et al.*[8] for Au. There are also dHvA data by Coleridge *et al.*[9] for Cu, by Joseph *et al.*[10] for Ag and by Bosacchi *et al.*[2] for Au. These data contain inconsistencies of the order of a few percent and it was the aim of this work to obtain a set of mass data for the three metals whose accuracy is better than 0.5%.

The paper is organized as follows. Section II is a short review of the theory of the dHvA effect as it pertains to the measurement of cyclotron masses and the subsequent determination of Fermi velocities and includes a discussion of electron-phonon interaction on the dHvA effect. In Sec. III the experimental setup is described in detail. Special emphasis is given to the temperature measurements and to the efforts made to avoid erroneous amplitude measurements as a consequence of skin effect. Section IV gives the experimental results for 54 extremal orbits in the planes {100} and {110}. In Sec. V, finally, local values for the Fermi velocities and for the electron-phonon enhancement factors are deduced from the data, and the coefficients of the electronic specific heat deduced from our dHvA data are compared with experimental results.

II. THEORY

A comprehensive review of the theory of the dHvA effect has been given by Gold,[11] so we restrict our attention to those aspects of the dHvA effect which relate to the measurements of cyclotron masses. The dHvA effect is the oscillatory variation of the magnetization M of the conduction electrons in a metal with the magnetic field H and can be expressed for one extremal cross section and no higher dHvA harmonics as

$$M = A(H, T, X^*)\sin(2\pi F/H + \beta)\,, \tag{1}$$

$$A = A_0(H, X^*)(bm_c^*T/m_0H)[\sinh(bm_c^*T/m_0H)]^{-1}\,, \tag{2a}$$

$$A_0 = D(H)\exp(-bm_c^*X^*/m_0H)\cos(\pi g_c^* m_c^*/2m_0)\,, \tag{2b}$$

$$D(H) = -\hbar e A_{ex}(4\pi^4 m_c^* c)^{-1}\left(\frac{2\pi eH}{\hbar c}\right)^{1/2}\left(\frac{\partial^2 A_{ex}}{\partial k_H^2}\right)^{-1/2}. \tag{2c}$$

m_0 is the free-electron mass, β is a phase constant, $F=\hbar cA_{ex}/2\pi e$ is the dHvA frequency, and A_{ex} is the extremal cross-sectional area of the Fermi surface. $b=2\pi^2 k_B c m_0/\hbar e$ has the value 14.69 TK^{-1}. m_c^*, X^*, and g_c^* are the cyclotron mass, the Dingle temperature, and the g factor for the orbit under consideration. Quantities marked by an asterisk are renormalized for electron-phonon interaction. Figure 1 illustrates the influence of electron-phonon interaction on the dHvA effect. The electron-phonon interaction changes the dispersion relation $E(\vec{k})$ of the conduction electrons in a range of width $k_B\Theta_D$ around the Fermi level[12] (Θ_D is the Debye temperature). In the vicinity of the Fermi level the dispersion relation reads

$$E^*(\vec{k})-E_F=[E(\vec{k})-E_F]/[1+\lambda(\vec{k})]. \tag{3}$$

$\lambda(\vec{k})$ is the well-known electron-phonon enhancement factor which is $\vec{k}$ dependent. As a consequence of this reduced slope the Fermi velocity $v^*(\vec{k})$ of the electrons is reduced by the factor $(1+\lambda)^{-1}$ compared to the band velocity $v(\vec{k})$

$$v^*(\vec{k})=v(\vec{k})/[1+\lambda(\vec{k})]. \tag{4}$$

The density of states $D^*(E_F)$ at the Fermi level is correspondingly increased. The difference between neighboring Landau levels is decreased by the factor $1/(1+\langle\lambda\rangle)$, where $\langle\lambda\rangle$ is the average of $\lambda(\vec{k})$ around the extremal orbit under consideration. Figure 1 illustrates the consequences of the changed dispersion relation Eq. (3) for the dHvA effect. The plot E^* vs E in the vicinity of E_F shows that the difference $\hbar\omega_c=\hbar eH/m_c c$ between neighboring Landau levels is reduced by the factor $1/(1+\langle\lambda\rangle)$ by electron-phonon interaction. The temperature damping of the dHvA amplitudes, which depends on the ratio of the Fermi surface smearing k_BT and the distance between neighboring Landau levels $\hbar\omega_c/(1+\langle\lambda\rangle)$, is therefore affected by electron-phonon interaction. In fact, it is the enhanced mass

$$m_c^*=m_c(1+\langle\lambda\rangle) \tag{5}$$

which enters into the temperature damping factor Eq. (2a). In cyclotron resonance transitions between neighboring Landau levels are induced by a rf field so that again it is the enhanced mass m_c^* which is measured by this technique. In contrast, the Dingle damping factor and the spin splitting factor, Eq. (2b), are not affected by electron-phonon interaction, because the Landau-level broadening and the spin splitting are reduced by the same factor $1/(1+\langle\lambda\rangle)$ as the Landau-level separation. Their ratio is therefore independent of this factor. This can be expressed in the following way:

$$m_c^*X^*=m_cX,\quad m_c^*g_c^*=m_cg_c\,. \tag{6}$$

The cyclotron masses m_c^* for different orbits were deduced from a measurement of the dHvA amplitude as a function of temperature T at fixed field H. According to Eq. (2a)

$$\ln\{(A/TA_0')[1-\exp(-2bm_c^*T/m_0H)]\}\,. \\ =-bm_c^*T/m_0H. \tag{7}$$

Neglecting the exponential on the left-hand side, the plot $\ln A/T$ vs T gave a first approximation to m_c^*. This value was inserted in the exponential of the left-hand side of Eq. (7) and the analysis redone giving the final value for m_c^*. In most cases the difference of m_c^* and its first approximation turned out to be negligible.

The cyclotron masses, defined by

$$m_c^*=\frac{\hbar^2}{2\pi}\left(\frac{\partial A}{\partial E}\right)^*, \tag{8}$$

are related to the local values of the Fermi velocity $v^*(\vec{k})$ by the following orbital average[13]:

$$m_c^*=\frac{\hbar}{2\pi}\oint d\alpha\,\frac{k_\perp^2}{(\hat{v}\cdot\vec{k}_\perp)}\,\frac{1}{v^*(\vec{k})}\,. \tag{9}$$

The weight function $k_\perp^2/(\hat{v}\cdot\vec{k}_\perp)$ depends only on the geometry of the Fermi surface. $\hat{v}$ denotes a unit vector along the gradient of the Fermi surface, and $\vec{k}_\perp$ is the radius vector of the extremal orbit. We have used the five coefficient symmetrized Fourier series of Halse[4] to calculate the weight functions in Eq. (9). Another five coefficient symmetrized Fourier series for the parametrization of the Fermi velocities $v^*(\vec{k})$ turned out to give only poor fits although the same type of function allows to fit the Fermi surface very well.[4] The reason is that the Fermi velocity is much more anisotropic than the Fermi surface. Trying to

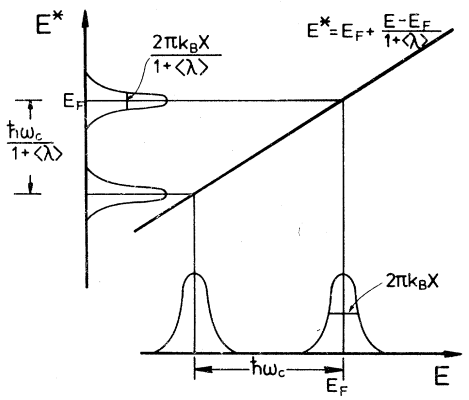

FIG. 1. Reduction of the Landau-level separation $\hbar\omega_c$ and broadening $2\pi k_BX$ by the factor $(1+\langle\lambda\rangle)^{-1}$ due to electron-phonon interaction.

keep the number of fitting parameters as small as possible, we have adopted the Fermi velocity parametrization chosen by Halse.[4] This scheme consists of constructing surfaces of constant energy adjacent to the Fermi surface and differing in energy from the Fermi energy by $\delta E/E_S = \pm 6\times 10^{-4}$. The difference is a factor of 10 smaller than that chosen by Halse. If δk is the distance between the surface $E_F - \delta E$ and the surface $E_F + \delta E$ at the point $\hat{\mathbf{k}}$ on the Fermi surface then the Fermi velocity in units of free-electron velocity v_s is

$$v^*(\hat{\mathbf{k}})/v_s = 6\times 10^{-4} k_s/\delta k . \tag{10}$$

Local values of the electron-phonon enhancement factor $1+\lambda(\hat{\mathbf{k}})$ can be obtained according to Eq. (4) if band velocities $v(\hat{\mathbf{k}})$ are known from a band-structure calculation. Another quantity of interest which can be deduced from the cyclotron masses is the coefficient of the electronic specific heat. If δV_k is the volume between the two surfaces $E_F \pm \delta E$, then γ^* in units of the free electron value γ_s is

$$\gamma^*\gamma_s = 10^4 \delta V_k/18 V_s . \tag{11}$$

III. EXPERIMENTAL

A. Experimental apparatus

The dHvA oscillations were measured with a standard field modulation technique.[14] To minimize skin effect a modulation frequency of 30 Hz was used. The signal induced in a balanced pickup coil was detected at twice the modulation frequency by means of a lock-in amplifier (PAR model 124). During the sweep of the magnetic field, the modulation field amplitude was continuously adjusted, to keep the Bessel function J_2 at its first maximum. The magnetic field was provided by a Nb-Ti superconducting solenoid with a field inhomogeneity of 3 parts in 10^6 over the specimen volume. The profile and the strength of the magnetic field were measured by means of an ^{27}Al NMR probe.[15] It turned out that the magnet has a hysteresis smaller than 5 G at 50 kG. For amplitude measurements we therefore used the magnet current as the field monitor with a conversion factor of 1.2180 kG/A. The field was swept linearly in $1/H$ to reduce errors in the amplitude measurements due to time constant effects in the signal detection electronics. A rotation mechanism allowed the sample to be turned through 360° around its cylinder axis. A tilt mechanism allowed the sample to be tilted by ±5 deg about an axis perpendicular to the rotation axis. We have used a combination of brass and plastic (Vespel SP1 by Dupond) to machine the sample holder. The coil formers and the tube containing the sample are made of Vespel. For gears combination of both were used. Since the two materials have very similar thermal expansion below room temperature very smooth rotation patterns of dHvA oscillations could be achieved. At symmetry directions the crystallographic direction of interest could be aligned by means of dHvA effect parallel to the magnetic field within a minute of arc. The alignment of the crystal for nonsymmetry orbits was made by linear interpolation of the angle settings for adjacent symmetry orbits.

B. Temperature measurements

The cryostat used consisted of an outer part containing the magnet and an inner part containing the sample holder. Any temperature between 1.1 and 4.2 K could be obtained by pumping the liquid ^{4}He in the inner cryostat. The sample and the sample holder were immersed in the liquid helium. On top of the magnet a helium reservoir (2.5 l, 13 cm inner diameter) was built into the inner cryostat to keep the liquid level fairly constant during a run. The sample temperature was determined by measuring the ^{4}He vapor pressure above the liquid using a capacitance manometer (Datametrics 521-12). For this purpose a stainless-steel tube of 3 mm inner diameter was inserted in the inner cryostat. Its open lower end was located in the helium reservoir above the liquid-helium level. At the lowest temperature used (1.17 K and 0.5 Torr) the mean free path of a helium atom in the gas is about 3 μm. Since this is small compared to the inner diameter of the tube, thermomolecular effects do not affect the pressure measurements. We have used the "1958 ^{4}He scale of temperature" to convert pressure readings into temperature readings. The absolute accuracy of the temperature measurement was checked at the λ point of helium ($T_\lambda = 2.172$ K) using the latent heat of the phase transition to monitor the pressure. The agreement was found to be better than 1 mK. The capacitance manometer output was connected to a temperature control unit which regulated a heater so that the bath temperature could be held constant within 1 mK for several hours. The poor heat conductivity of normal helium and the strongly temperature-dependent specific weight of helium made it necessary to install the heater below the sample. The temperature dependence of the dHvA amplitudes was measured at decreasing helium temperatures to make sure that the liquid was in thermal equilibrium with its vapor. The sample was placed some 20 cm below the helium-liquid level. The hydrostatic pressure of the liquid changed its boiling point at the sample position compared to the

liquid surface. This effect required a pressure correction for temperatures above 2.172 K. The details of this correction will be explained below.

C. Single crystals

All single crystals used in this investigation were grown by the Czochralski technique as wires 1 mm in diameter and about 100 mm in length.[16] They were cut by an acid layer saw in pieces about 5 mm in length.[17] No spark erosion was applied. No further heat treatment was applied to the Cu and Ag crystals. Typical Dingle temperatures were about 30 mK for all orbits. On the other hand the Au crystals improved substantially by annealing them in air at 970 °C for 3 h in alumina crucibles and cooling down the furnace over night. Prior to the heat treatment the Dingle temperatures were 200 mK for the belly orbits, and 500 mK for the neck and dogsbone orbit, decreasing to 30 mK after the heat treatment. The copper and gold single crystals had dislocation densities as low as 1000, respectively, 2000/cm^2. The residual resistivity of the samples was 0.5, 0.5, and 0.4 nΩ cm for Cu, Ag, and Au, respectively.

IV. EXPERIMENTAL RESULTS

Figure 2 shows three plots $\ln(A/T)$ vs T according to Eq. (7) for a Cu, Ag, and Au orbit with the deduced values for the cyclotron masses m_c^*. B, R, N, and D denote belly, rosette, neck, and dogsbone. The numbers following these symbols indicate the angle in degrees by which the orbit under consideration is tilted against the direction ⟨100⟩. The copper data show how the temperature correction due to the hydrostatic pressure of the helium above the sample is made. The measured values above T_λ are characterized by crosses. First a least-squares fit is made through the points measured below T_λ. Then the lowest point above T_λ is shifted in temperature, so that it coincides with the least-squares fit. To the temperature shift corresponds a helium vapor pressure that is now added to all the vapor-pressure measurements above T_λ. The final temperatures are calculated from these corrected vapor pressures. The final values $\ln(A/T)$ vs T are indicated by circles in Fig. 2. The measurement above T_λ without the temperature correction gave for the Cu belly saddle point (BSP) of Fig. 2 a cyclotron mass of $(1.286 \pm 0.005)m_0$. This has to be compared to the corrected value of $(1.320 \pm 0.003)m_0$. The difference between these two values is much larger than the errors quoted, which are rms errors of the least-squares fit. It turned out that the pressure corrections were in all cases nearly 2 Torr as a consequence of the stable helium level above the sample of about 20 cm during a run. Therefore we have added 2 Torr as well to all pressure readings in those cases where we have made no measurements below the λ point. Especially in the case of silver no belly measurements were made below T_λ due to the problem of magnetic interaction.

Magnetic interaction can be a serious source of systematic errors for the amplitude measurements. We have chosen the field and temperatures values for each orbit in such a way that this effect

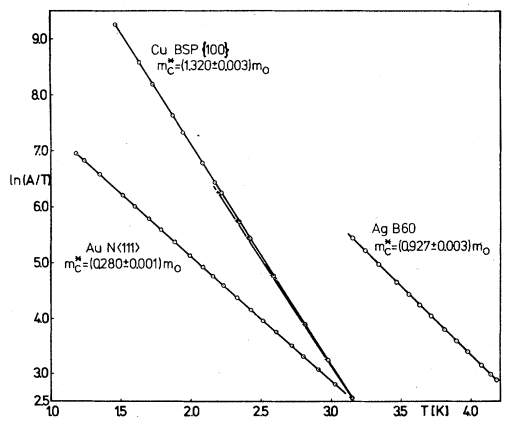

FIG. 2. Temperature dependence of the dHvA amplitudes for three different orbits in Cu, Ag, and Au. The slope of the lines is proportional to the cyclotron mass m_c^* renormalized by the electron-phonon interaction. The Cu data show the influence of the hydrostatic pressure of helium above the sample on the temperature reading above T_λ. (BSP: belly saddle-point orbit in the plane {100}.)

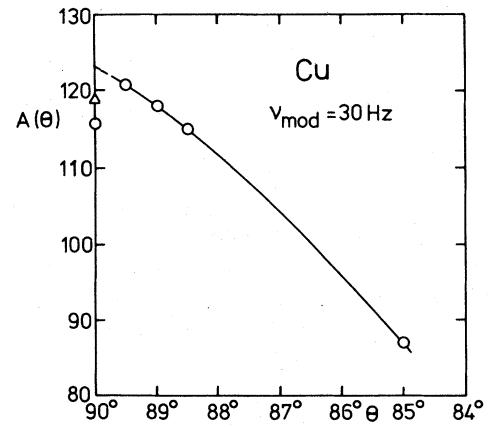

FIG. 3. Influence of incomplete penetration of the modulation field into the sample on the dHvA amplitude. Owing to skin effect the dogsbone amplitude (Θ = 90°) is too small. The circles and the triangle denote the amplitudes for those lock-in phase settings which maximize the amplitude at Θ = 85°, respectively, Θ = 90°.

TABLE I. Cyclotron masses measured by dHvA effect in Cu, Ag, and Au. The notation describing orbits and orientations is the following: B, R, N, and D denote belly, four-cornered rosette, neck, and dogsbone orbits. The angles Θ and Φ are from [001] in the $\{110\}$ and $\{100\}$ planes, respectively. The numbers behind the symbols give the angle between the magnetic field and the crystallographic direction [001] (Θ in the plane $\{110\}$ and Φ in the plane $\{100\}$). The errors quoted are rms errors of the least-squares fit to the data according to Eq. (7). The masses calculated from the fitted surfaces $C^{\pm}_{lmn}$ agree within the rms errors with the measured ones.

	Experiment	$C^{\pm}_{lmn}$		Experiment	$C^{\pm}_{lmn}$
	(a) Cu			(b) Ag	
$\{110\}$			B 65	0.954 ± 0.003	0.953
$B\langle 100\rangle$		1.341	$R\langle 100\rangle$	1.044 ± 0.004	1.044
B 0.5	1.343 ± 0.004	1.341	$N\langle 111\rangle$	0.365 ± 0.001	0.366
B 10	1.315 ± 0.002	1.317	N 60	0.375 ± 0.001	0.374
BTP 16.2	1.310 ± 0.003	1.309	D 85	1.030 ± 0.002	1.031
B 50	1.388 ± 0.003	1.391	$D\langle 110\rangle$	1.001 ± 0.002	1.000
$B\langle 111\rangle$	1.378 ± 0.003	1.375	$\{100\}$		
B 65	1.431 ± 0.004	1.433	B 4	0.933 ± 0.002	0.932
$R\langle 100\rangle$		1.306	B 7	0.923 ± 0.002	0.925
R 0.5	1.307 ± 0.002	1.306	BSP 13.6	0.912 ± 0.002	0.912
$N\langle 111\rangle$	0.444 ± 0.001	0.444			
N 65	0.478 ± 0.002	0.480		(c) Au	
N 75	0.648 ± 0.004	0.645	$\{110\}$		
D 85	1.288 ± 0.004	1.287	$B\langle 100\rangle$		1.142
D 89.5	1.260 ± 0.002	1.262	B 1	1.140 ± 0.004	1.141
$D\langle 110\rangle$		1.262	B 5	1.121 ± 0.003	1.122
$\{100\}$			B 10	1.084 ± 0.002	1.083
B 7	1.326 ± 0.003	1.328	B 15	1.051 ± 0.003	1.050
BSP 11.8	1.320 ± 0.003	1.319	B 23	1.052 ± 0.002	1.053
B 18	1.327 ± 0.004	1.325	B 50	1.074 ± 0.005	1.074
B 29.2	1.468 ± 0.005	1.468	$B\langle 111\rangle$	1.066 ± 0.002	1.065
D 40	1.309 ± 0 004	1.309	B 60	1.071 ± 0.002	1.072
	(b) Ag		$R\langle 100\rangle$		1.014
$\{100\}$			R 1	1.014 ± 0.004	1.014
$B\langle 100\rangle$	0.938 ± 0.003	0.936	$N\langle 111\rangle$	0.280 ± 0.001	0.281
B 7	0.923 ± 0.002	0.924	N 60	0.286 ± 0.001	0.286
B 8	0.919 ± 0.002	0.921	D 85	1.003 ± 0.003	1.003
B 10	0.916 ± 0.003	0.915	D 89.5	0.983 ± 0.002	0.983
B 12	0.911 ± 0.002	0.909	$D\langle 110\rangle$		0.983
BTP 18.4	0.904 ± 0.003	0.903	$\{100\}$		
B 24	0.934 ± 0.002	0.934	B 8	1.107 ± 0.002	1.106
B 50	0.928 ± 0.002	0.929	BSP 16.3	1.067 ± 0.002	1.067
$B\langle 111\rangle$	0.923 ± 0.003	0.920	B 25	1.073 ± 0.003	1.072
B 60	0.927 ± 0.003	0.929	D 40	1.018 ± 0.003	1.018

could be neglected. A source of systematic errors in the mass measurement much harder to avoid in our high quality single crystals turned out to be the inhomogeneous penetration of the modulation field into the samples. At a modulation frequency of 30 Hz the classical skin depth is below 0.5 mm. The magnetoresistance of the samples increases the skin depth substantially so that for most orbits a frequency of 30 Hz was low enough, except for the belly $\langle 100\rangle$ and the dogsbone $\langle 110\rangle$ orbits, where magnetoresistance is especially low. We found out that the phase setting at the lock-in amplifier for maximum dHvA amplitude was independent of the orbit and independent of the material (Cu, Ag, or Au) if skin effect does not affect the amplitudes. This was fulfilled with our setup for all orbits investigated except for the $B\langle 100\rangle$ and the $D\langle 110\rangle$ orbit. Figure 3 is a plot of the amplitudes of the dHvA oscillations in Cu as a function of the angle Θ in the plane $\{110\}$ near the dogsbone orbit ($\Theta = 90°$). The phase setting of the lock-in was chosen so that the amplitude of the orbit $\Theta = 85°$ was maximized. This same phase setting maximized also the amplitudes of the other orbits except that of the symmetry direction $\Theta = 90°$, which is obviously too low. This is a consequence of skin effect. It should be noted that the orbit $\Theta = 89.5°$ is not affected by skin effect.

TABLE II. Values of the coefficients C_{lmn} and $C^{\pm}_{lmn}$ in the symmetrized Fourier series representations of the surfaces of constant energy for Cu, Ag, and Au. The values C_{lmn} for the Fermi surface are taken from Halse (Ref. 4). The energies of the neighboring surfaces $C^{\pm}_{lmn}$ differ from the Fermi energy by $\delta E/E_s = 6\times10^{-4}$. Q is the quality factor of the fit defined by Eq. (14).

	C_{000}	C_{200}	C_{211}	C_{220}	C_{310}	Q
Cu5	1.691 67	0.006 93	−0.425 01	−0.016 79	−0.037 72	
Cu5+	1.705 924 66	0.007 729 89	−0.422 118 86	−0.016 660 28	−0.037 676 56	2.46×10^{-3}
Cu5−	1.680 147 19	0.006 285 05	−0.427 344 80	−0.016 833 75	−0.037 727 87	2.63×10^{-3}
Ag5	−0.897 89	−0.120 30	−0.901 87	−0.140 86	−0.094 83	
Ag5+	−0.872 822 92	−0.118 933 92	−0 896 994 63	−0.140 174 56	−0.094 589 95	1.63×10^{-3}
Ag5−	−0 911 863 67	−0.121 069 83	−0.904 572 99	−0.141 141 57	−0.094 880 56	1.66×10^{-3}
Au5	−2.262 13	−0.166 35	−1.255 16	−0.099 14	−0.127 04	
Au5+	−2.385 641 06	−0.172 520 43	−1.280 091 38	−0.102 874 77	−0.129 761 67	0.91×10^{-3}
Au5−	−2.141 185 39	−0.160 307 68	−1 230 744 33	−0.095 483 86	−0.124 377 59	0.78×10^{-3}

A shift of the lock-in phase by 16°, maximizing the $D\langle110\rangle$ amplitude increases the amplitude by 2.6% (triangle in Fig. 3). The amplitude is still smaller than the amplitude extrapolated from the orbits $\Theta \neq 90°$. We finally overcame the problem of skin effect in our samples by measuring the masses for the orbits B 0.5, R 0.5, B 1, R 1, and D 89.5 instead of the orbits $B\langle100\rangle$, $R\langle100\rangle$, and $D\langle110\rangle$ themselves. In addition, we have quenched-in some 80 ppm of lattice vacancies in a Ag crystal, increasing the residual resistivity by about 8 nΩ cm,[18] which was enough to measure the masses exactly at symmetry directions without skin-effect problems. Table I is a compilation of the data obtained for the three metals. The errors quoted are rms errors of the least-squares fits. All masses were measured at least two times and in each run the amplitudes were measured for at least 12 different temperatures. When the sources of systematic errors mentioned above were eliminated the data were reproducible within the errors quoted in the table.

TABLE III. Cyclotron masses in Cu, Ag, and Au calculated from the surfaces $C^{\pm}_{lmn}$ given in Table II. The angles Θ and Φ are from [001] in the planes $\{110\}$ and $\{100\}$.

	Cu	Ag	Au		Cu	Ag	Au
$B\,\Theta=0$	1.341	0.936	1.142	$D\,\Theta=90$	1.262	1.000	0.983
5	1.333	0.930	1.122	88	1.266	1.005	0.986
10	1.317	0.915	1.083	85	1.287	1.031	1.003
15	1.308	0.903	1.050	83	1.313	1.066	1.025
20	1.325	0.907	1.038	80	1.377	1.178	1.078
25	1.481	0.949	1.096	78	1.446	···	1.137
26	1.714	0.970	1.207	$D\,\Phi=43$	1.269	1.009	0.988
27.5	···	1.035	1.426	40	1.309	1.065	1.018
45	1.664	0.977	1.165	37.5	1.381	1.218	1.075
47	1.441	0.949	1.098	35	1.541	···	1.217
50	1.391	0.929	1.074	$R\,\Theta=0$	1.306	1.044	1.014
54.74	1.375	0.920	1.065	5	1.417	1.218	1.102
60	1.388	0.929	1.072	$N\,\Theta=30$	0.952	0.849	0.576
65	1.433	0.953	1.095	32	0.774	0.662	0.478
70	1.558	1.004	1.155	35	0.638	0.534	0.398
73	2.013	1.061	1.286	40	0.529	0.438	0.333
$B\,\Phi=5$	1.333	0.930	1.124	45	0.476	0.393	0.300
10	1.322	0.918	1.094	50	0.451	0.372	0.285
15	1.319	0.911	1.071	54.74	0.444	0.366	0.281
20	1.333	0.917	1.061	60	0 453	0 374	0.286
25	1.377	0.941	1.072	65	0.480	0.397	0.303
30	1.500	0.998	1.130	70	0.534	0.444	0.336
32	1.653	1.041	1.199	75	0.645	0.546	0.404
33	1.956	1.072	1.282	77	0.722	0.624	0.450

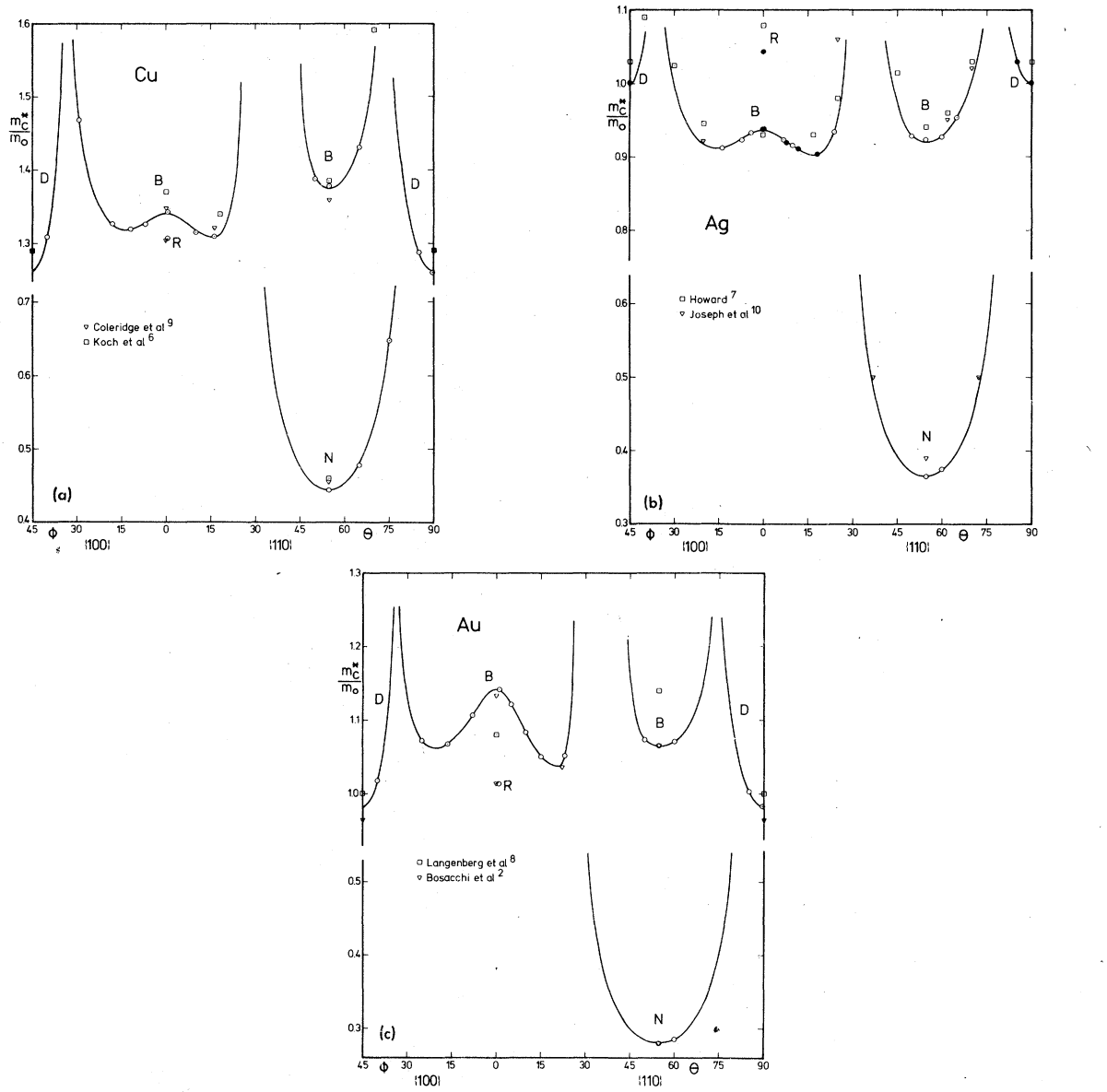

FIG. 4. (a)–(c) Orientation dependence of the cyclotron masses in Cu, Ag, and Au in the planes {110} and {100} as calculated from the two surfaces $C^{\pm}_{lmn}$. Circles denote our data from Table I. The full circles in the case of Ag were measured on the sample containing some 80 ppm of lattice vacancies. Squares denote cyclotron resonance data by Koch *et al.* (Ref. 6) for Cu, by Howard (Ref. 7) for Ag, and by Langenberg *et al.* (Ref. 8) for Au. The triangles denote dHvA data by Coleridge *et al.* (Ref. 9) for Cu, by Joseph *et al.* (Ref. 10) for Ag, and by Bosacchi *et al.* (Ref. 2) for Au.

V. DATA ANALYSIS AND DISCUSSION

The experimental data for the cyclotron masses given in Table I have been analyzed as described in Sec. II. We have first constructed two surfaces of constant energy differing by $\delta E/E_s = \pm 6 \times 10^{-4}$ from the Fermi energy. The surfaces of constant energy were represented by symmetrized Fourier series of the form

$$C_0 = 3 - \sum \cos\tfrac{1}{2}ak_x \cos\tfrac{1}{2}ak_y + C_{200}\left(3 - \sum \cos ak_x\right) + C_{211}\left(3 - \sum \cos ak_x \cos\tfrac{1}{2}ak_y \cos\tfrac{1}{2}ak_z\right)$$

$$+ C_{220}\left(3 - \sum \cos ak_x \cos ak_y\right) + C_{310}\left(6 - \sum \cos\tfrac{3}{2}ak_x \cos\tfrac{1}{2}ak_y - \sum \cos\tfrac{1}{2}ak_x \cos\tfrac{3}{2}ak_y\right), \qquad (12)$$

TABLE IV. Fermi velocities in units v_s for Cu, Ag, and Au. ϑ and φ denote the polar angles with the pole at [001]. The values v^*/v_s at the neck are (0.425 ± 0.001), (0.371 ± 0.001), and (0.638 ± 0.002) for Cu, Ag, and Au, respectively.

	φ 0	5	10	15	20	25	30	35	40	45
(a) Cu										
ϑ 0	0.684	0.684	0.684	0.684	0.684	0.684	0.684	0.684	0.684	0.684
5	0.727	0.727	0.727	0.727	0.727	0.727	0.727	0.727	0.727	0.727
10	0.790	0.790	0.790	0.790	0.790	0.790	0.790	0.790	0.790	0.790
15	0.813	0.813	0.813	0.813	0.814	0.814	0.814	0.815	0.815	0.815
20	0.800	0.800	0.801	0.803	0.804	0.806	0.808	0.809	0.810	0.810
25	0.772	0.773	0.775	0.778	0.782	0.785	0.788	0.791	0.792	0.793
30	0.743	0.744	0.747	0.752	0.757	0.763	0.767	0.770	0.771	0.772
35	0.718	0.720	0.724	0.730	0.736	0.742	0.744	0.744	0.741	0.740
40	0.702	0.704	0.708	0.715	0.720	0.721	0.714	0.696	0.674	0.664
45	0.696	0.698	0.703	0.709	0.711	0.700	0.664	0.585	0.477	0.428
50	0.702	0.704	0.708	0.713	0.711	0.685	0.600	...	...	...
55	0.718	0.720	0.724	0.727	0.722	0.689	0.581	...	...	...
60	0.743	0.744	0.747	0.748	0.741	0.714	0.634	0.439	...	...
65	0.772	0.773	0.773	0.771	0.763	0.742	0.701	0.625	0.522	0.464
70	0.800	0.800	0.798	0.792	0.781	0.763	0.739	0.709	0.680	0.667
75	0.813	0.814	0.813	0.807	0.793	0.773	0.752	0.731	0.715	0.708
80	0.790	0.799	0.813	0.814	0.798	0.775	0.750	0.728	0.713	0.708
85	0.727	0.756	0.799	0.814	0.800	0.773	0.745	0.721	0.705	0.700
90	0.684	0.727	0.790	0.813	0.800	0.772	0.743	0.718	0.702	0.696
(b) Ag										
ϑ 0	0.927	0.927	0.927	0.927	0.927	0.927	0.927	0.927	0.927	0.927
5	0.976	0.976	0.976	0.976	0.976	0.976	0.976	0.976	0.976	0.976
10	1.067	1.067	1.067	1.067	1.068	1.068	1.068	1.069	1.069	1.069
15	1.129	1.129	1.130	1.131	1.133	1.134	1.136	1.137	1.138	1.138
20	1.145	1.146	1.148	1.151	1.155	1.159	1.162	1.165	1.167	1.168
25	1.132	1.133	1.136	1.141	1.147	1.153	1.159	1.163	1.166	1.167
30	1.106	1.108	1.112	1.118	1.125	1.131	1.136	1.139	1.141	1.141
35	1.081	1.082	1.087	1.092	1.097	1.100	1.098	1.092	1.087	1.084
40	1.063	1.064	1.068	1.071	1.071	1.061	1.039	1.007	0.975	0.962
45	1.056	1.058	1.061	1.061	1.051	1.021	0.957	0.855	0.740	0.683
50	1.063	1.064	1.067	1.064	1.046	0.992	0.872	0.638	...	...
55	1.081	1.082	1.085	1.083	1.061	0.997	0.850	0.529	...	...
60	1.106	1.108	1.112	1.111	1.092	1.037	0.919	0.699	...	...
65	1.132	1.135	1.140	1.141	1.127	1.088	1.016	0.907	0.785	0.725
70	1.145	1.150	1.159	1.164	1 154	1.127	1.084	1.031	0.982	0.962
75	1.129	1.138	1.158	1.170	1.165	1.144	1.113	1.080	1.053	1.043
80	1.067	1.087	1.129	1.158	1.161	1.143	1.116	1.089	1.068	1.061
85	0.976	1.014	1.087	1.138	1.151	1.136	1.110	1.084	1.065	1.059
90	0.927	0.976	1.067	1.129	1.145	1.132	1.106	1.081	1.063	1.056
(c) Au										
ϑ 0	0.736	0.736	0.736	0.736	0.736	0.736	0.736	0.736	0.736	0.736
5	0.891	0.891	0.891	0.891	0.891	0.891	0.891	0.891	0.891	0.891
10	1.014	1.014	1.015	1.015	1.017	1.018	1.019	1.020	1.021	1.021
15	1.028	1.029	1.031	1.035	1.040	1.045	1.050	1.054	1.057	1.058
20	0.997	0.999	1.004	1.013	1.023	1.034	1.045	1.054	1.061	1.063
25	0.952	0.955	0.963	0.976	0.993	1.012	1.030	1.046	1.056	1.059
30	0.905	0.909	0.920	0 938	0.961	0.987	1.012	1.034	1.048	1.053
35	0.866	0.870	0.884	0.906	0.934	0.964	0.993	1.016	1.030	1.035
40	0.839	0.845	0.860	0.885	0.915	0.946	0.970	0.978	0.974	0.969
45	0.830	0.836	0.853	0.879	0.910	0.934	0.931	0.872	0.757	0.690

TABLE IV. (*Continued*)

	φ 0	5	10	15	20	25	30	35	40	45
(c) Au										
50	0.839	0.846	0.865	0.893	0.922	0.934	0.878	0.640	•••	•••
55	0.866	0.873	0.894	0.924	0.953	0.956	0.868	•••	•••	•••
60	0.905	0.913	0.936	0.967	0.994	0.998	0.935	0.708	•••	•••
65	0.952	0.960	0.983	1.012	1.033	1.035	1.002	0.923	0.806	0.737
70	0.997	1.006	1.026	1.047	1.055	1.045	1.017	0.979	0.942	0.925
75	1.028	1.036	1.054	1.062	1.053	1.026	0.990	0.954	0.927	0.916
80	1.014	1.031	1.055	1.055	1.031	0.993	0.950	0.911	0.884	0.874
85	0.891	0.961	1.031	1.037	1.007	0.963	0.917	0.878	0.851	0.842
90	0.736	0.891	1.014	1.028	0.997	0.952	0.905	0.866	0.839	0.830

using the lattice parameters a and the coefficients C_{lmn} for the Fermi surface given by Halse.[4] We denote by $C^{\pm}_{lmn}$ the coefficients characterizing the two neighboring surfaces with energies $E_s \pm \delta E$. If A^+, A^-, and A_{ex} are the extremal cross-sectional areas of these two surfaces and of the Fermi surface for a given field direction, then according to Eq. (8) it is

$$\frac{m_c^*}{m_0} = \frac{(A^{\pm} - A_{ex})}{\pi k_s^2} \frac{E_s}{\delta E} . \tag{13}$$

$k_s = (12\pi^2)^{1/3}/a$ is the free-electron Fermi-surface radius. The coefficients $C^{\pm}_{lmn}$ were determined in such a way that the areas $A^{\pm}$ fitted the measured masses according to Eq. (13). All the masses of Table I were used in the fitting procedure which was done by means of the nonlinear least-squares-fitting program VA 05 AD from the Harwell Subroutine Library. The quality of the fit can be expressed by

$$Q = \left\{ \frac{1}{N-5} \sum_{i=1}^{N} \left[\left(\frac{m_{ci}^*}{m_0} \right)_{\text{exp}} - \frac{A_i^{\pm} - A_{ex\,i}}{\pi k_s^2} \frac{E_s}{\delta E} \right]^2 \right\}^{1/2} , \tag{14}$$

where N is the number of fitted masses. The values of the fitted parameters $C^{\pm}_{lmn}$ are given in Table II. The masses calculated from the surfaces C^{+}_{lmn} and C^{-}_{lmn} are compared to the experimental data in Table I. The fitted masses agree within the experimental accuracy with the measured data. This is expressed by the low-Q values in Table I as well.

One of the applications of the $C^{\pm}_{lmn}$ surfaces has been in the calculation of masses which were not measured. Table III gives a list of some masses for orbits in the planes {110} and {100}. Figures 4(a)–4(c) show the orientation dependence of the calculated cyclotron masses. The experimental data used in the fits are characterized by circles. For comparison some of the most recent cyclotron resonance and dHvA data are shown as well.

Another application of the surfaces $C^{\pm}_{lmn}$ is the calculation of local values of the Fermi velocities according to Eq. (10). Computed velocities over a 5° grid for Cu, Ag, and Au are given in Table IV, parts a–c. The velocities are expressed in free-electron velocity units v_s. The data are re-

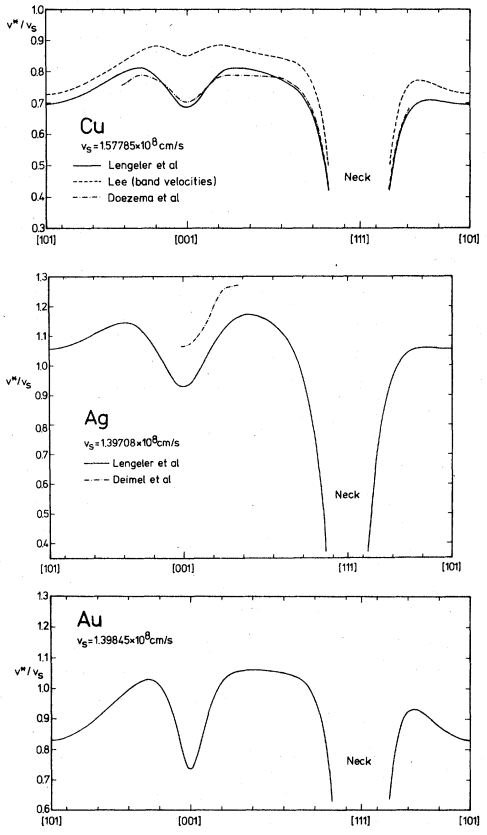

FIG. 5. (a)–(c) Fermi velocities in Cu, Ag, and Au in units of free-electron velocities v_s. Solid line: our result; dot-dashed line: from magnetic surface states; dashed line: band velocities for Cu by Lee (Ref. 21).

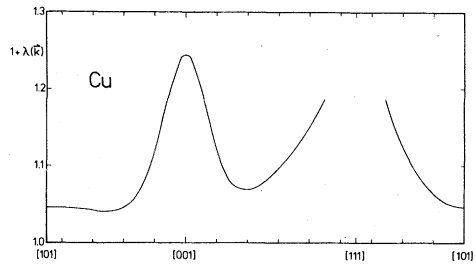

FIG. 6. Local values of the electron-phonon enhancement factor $1+\lambda(\hat{k})$ for Cu.

liable to better than 1% especially in the neck region where the accuracy is 0.3%. Values of the Fermi velocities for some high-symmetry directions in Cu, Ag, and Au drawn from Table IV are shown in the Figs. 5(a)–5(c). For Cu Doezema and Koch[19] have determined Fermi velocities from resonance spectra of magnetic-field-induced surface states. Their data shown in Fig. 5(a) have an accuracy of ±1.5%. Near the belly point [100] the discrepancies with our data are somewhat larger than the errors quoted, whereas at the neck the agreement is excellent. For Ag Deimel and Doezema[20] have determined Fermi velocities from magnetic surface states spectra. Their results which have an accuracy of ±3% are shown in Fig. 5(b) and are substantially higher than our results. Since 13 of the 20 masses used in the construction of the surfaces $C^{\pm}_{lmn}$ cover the point [100] and its vicinity we believe that our velocities should be especially accurate in this region of the Fermi surface. The velocities obtained by Halse[4] from his neighboring surfaces $C^{\pm}_{lmn}$ agree with our data within the errors quoted (0.03 v_s for his Cu and Ag data and 0.10 v_s for his Au data).

Lee[21] has calculated band velocities for Cu from a one-electron potential that has been constructed to fit optical and Fermi-surface data. We have used our velocities from Table IV and these band velocities which are shown in Fig. 5(a) to compute local values of the electron-phonon enhancement factor $1+\lambda(\hat{k})$ according to Eq. (4). The result is shown in Fig. 6. $\lambda(\hat{k})$ is markedly anisotropic over the Fermi surface reaching maxima at the necks and at the belly points ⟨100⟩. No experimental data of the $\hat{k}$ dependence of $1+\lambda$ are available at present time. However, values of the average of $\lambda(\hat{k})$ over the Fermi surface have been measured by Hoyt and Mota[22] ($\bar{\lambda}=0.16$) and by Chaikin and Hansma[23] ($\bar{\lambda}=0.13\pm0.03$). Calculated values of $\bar{\lambda}$ are 0.15 by Teichler,[24] 0.15 ± 0.02 by Das,[25] 0.12 ± 0.02 by Nowak,[26] and 0.14 by Grimvall.[27]

The mean value deduced from our data is $\bar{\lambda}=0.11$. This is somewhat smaller than the values quoted above. In view of the limited accuracy of the calculated band velocities underlying our values of λ this discrepancy is not significant.

TABLE V. Coefficients of electronic specific heat γ^* in free-electron units γ_s for Cu, Ag, and Au, as calculated from this work and others compared to the measured values of Martin.

	γ^*/γ_s	
Cu	1.382 ± 0.010	This work
	1.383 ± 0.002	Martin (Ref. 28)
	1.397 ± 0.016	Bosacchi *et al.* (Ref. 29)
	1.400	Halse (Ref. 4)
Ag	1.008 ± 0.007	This work
	1.004 ± 0.002	Martin (Ref. 28)
	1.021	Halse (Ref. 4)
Au	1.074 ± 0.007	This work
	1.083 ± 0.002	Martin (Ref. 28)
	1.077	Bosacchi *et al.* (Ref. 2)
	1.093	Halse (Ref. 4)

The coefficient γ^* of the electronic specific heat was calculated from the volume between the two surfaces $C^{\pm}_{lmn}$. Table V gives a list of the values of γ^* in units of the free-electron value γ_s. For comparison the values of $\gamma^*\gamma_s$ by Martin[28] from specific-heat measurements are shown as well. These are probably the most reliable data known at present time. The agreement with our data is excellent, especially for Cu and Ag.

VI. CONCLUSIONS

The temperature dependence of the dHvA amplitudes is one of the most powerful tools for the determination of cyclotron masses in metals. For the noble metals Cu, Ag, and Au investigated here, the accuracy of the data has been substantially increased compared to that of previous dHvA measurements and of the cyclotron resonance data available at present time. This is a consequence of the successful elimination of systematic errors in the temperature and in the amplitude determination. Mass data deduced from cyclotron resonance by means of Azbel-Kaner theory are correct only if the magnetic field is aligned accurately parallel to the surface of the sample.[6] Even small tip angles as produced for instance by surface roughness can seriously affect the accuracy of the data. These problems do not occur in dHvA measurements.

Another advantage of the dHvA technique is the ability to accurately orient the crystal in the magnetic field by using the dHvA effect itself. Local values of the Fermi velocities can be calculated from the measured cyclotron masses by a deconvolution procedure which requires a correct knowledge of the Fermi surface. In the case of

the noble metals whose Fermi surfaces are among the best known this deconvolution has been achieved successfully. On the other hand nearly local values of the Fermi velocities are obtained without further deconvolution from the resonance spectra of magnetic surface states. This is a great advantage especially in metals with a more complicated Fermi surface. But the high requirement on the sample purity and on the surface preparation restrict this method to a rather small number of metals. In the case of Cu where the problems of sample preparation have been solved the velocities determined by dHvA effect and by magnetic surface states are in good agreement. This is not the case for Ag, where the surface preparation causes much greater problems than for Cu.[20] In Au no magnetic surface states have been observed till now.

ACKNOWLEDGMENT

The authors would like to thank J. Keppels for technical assistance during the measurements.

*Present address: Sandia Laboratories, Albuquerque, N.M. 87115.

†Permanent address: University of Oklahoma, Dept. of Physics and Astronomy, Norman, Oklahoma 73069.

[1]A. P. Cracknell, *The Fermi Surface of Metals* (Taylor and Francis, London, 1971), pp. 145–156.

[2]B. Bosacchi, J. B. Ketterson, and L. R. Windmiller, Phys. Rev. B 4, 1197 (1971).

[3]P. T. Coleridge and I. M. Templeton, J. Phys. F 2, 643 (1972).

[4]M. R. Halse, Philos. Trans. R. Soc. Lond. 265, 507 (1969).

[5]M. Springford, Adv. Phys. 20, 493 (1971).

[6]J. F. Koch, R. A. Stradling, and A. F. Kip, Phys. Rev. 133, A240 (1964).

[4]D. G. Howard, Phys. Rev. 140, A1705 (1965).

[8]D. N. Langenberg and S. M. Marcus, Phys. Rev. 136, A1383 (1964).

[9]P. T. Coleridge and B. R. Watts, Can. J. Phys. 49, 2379 (1971).

[10]A. S. Joseph and A. C. Thorsen, Phys. Rev. 138, A1159 (1965).

[11]A. V. Gold, in *Solid State Physics*, edited by J. F. Cochran and R. R. Haering (Gordon and Breach, New York, 1968), Vol. I.

[12]J. W. Wilkins, *Observable Many-Body Effects in Metals* (Nordita, Copenhagen, 1968).

[13]D. H. Lowndes, K. M. Miller, R. G. Poulsen, and M. Springford, Proc. R. Soc. A 331, 497 (1973).

[14]L. R. Windmiller and J. R. Ketterson, Rev. Sci. Instrum. 39, 1672 (1968).

[15]W. R. Wampler, S. Matula, G. Durcansky, and B. Lengeler, Rev. Sci. Instrum. 46, 58 (1975).

[16]H. Fehmer and W. Uelhoff, J. Cryst. Growth 13/14, 257 (1972).

[17]M. Abdel Fattah, V. Sorajic, and W. Uelhoff, Berichte der KFA-Jülich, JÜL-944-FF (1973) (unpublished).

[18]B. Lengeler, Philos. Mag. 34, 259 (1976).

[19]R. E. Doezema and J. F. Koch, Phys. Rev. B 5, 3866 (1972).

[20]P. Deimel and R. E. Doezema, Phys. Rev. B 10, 4897 (1974).

[21]M. J. G. Lee, Phys. Rev. B 2, 250 (1970).

[22]R. F. Hoyt and A. C. Mota, Solid State Commun. 18, 138 (1976).

[23]P. M. Chaikin, P. K. Hansma, Phys. Rev. Lett. 36, 1552 (1976).

[24]H. Teichler, Phys. Status Solidi B 48, 189 (1971).

[25]S. G. Das, Phys. Rev. B 7, 2238 (1973).

[26]D. Nowak, Phys. Rev. B 6, 3691 (1972).

[27]G. Grimvall, Phys. Kondens. Mater. 14, 101 (1972).

[28]D. L. Martin, Phys. Rev. B 8, 5357 (1973).

[29]B. Bosacchi and P. Franzosi, Phys. Rev. B 12, 5999 (1975).